Draft version December 21, 2011
Preprint typeset using LaTeX style emulateapj v. 5/2/11

SLAC-PUB-14849

MAGNETIC FIELDS IN POPULATION III STAR FORMATION

Matthew J. Turk[1,2], Jeffrey S. Oishi[3,4], Tom Abel[3,4], Greg L. Bryan[1]

Draft version December 21, 2011

ABSTRACT

We study the buildup of magnetic fields during the formation of Population III star-forming regions, by conducting cosmological simulations from realistic initial conditions and varying the Jeans resolution. To investigate this in detail, we start simulations from identical initial conditions, mandating 16, 32 and 64 zones per Jeans length, and studied the variation in their magnetic field amplification. We find that, while compression results in some amplification, turbulent velocity fluctuations driven by the collapse can further amplify an initially weak seed field via dynamo action, provided there is sufficient numerical resolution to capture vortical motions (we find this requirement to be 64 zones per Jeans length, slightly larger than, but consistent with previous work run with more idealized collapse scenarios). We explore saturation of amplification of the magnetic field, which could potentially become dynamically important in subsequent, fully-resolved calculations. We have also identified a relatively surprising phenomena that is purely hydrodynamic: the higher-resolved simulations possess substantially different characteristics, including higher infall-velocity, increased temperatures inside 1000 AU, and decreased molecular hydrogen content in the innermost region. Furthermore, we find that disk formation is suppressed in higher-resolution calculations, at least at the times that we can follow the calculation. We discuss the effect this may have on the buildup of disks over the accretion history of the first clump to form as well as the potential for gravitational instabilities to develop and induce fragmentation.

Subject headings: cosmology: theory — galaxies: formation — galaxies: HII regions — stars: formation

1. INTRODUCTION

The formation of the first stars in the Universe is a process well-suited to numerical computation. While direct observations of these stars are still an optimistic, yet-unrealized prospect (Wise & Abel 2005; Frost et al. 2009; Frebel et al. 2005; Caffau et al. 2011), simulations are able to begin with well-posed initial conditions and directly simulate their formation. These calculations, typically spanning many orders of magnitude in both spatial and density scales (Turk et al. 2008; Yoshida et al. 2008), include the effects of dark matter, hydrodynamics, radiative cooling, chemical heating and cooling, and the non-equilibrium, self-consistent evolution of multiple ionization and molecular states of the gas (Abel et al. 1997; Anninos et al. 1997; Ripamonti & Abel 2004; Glover 2008; Glover & Abel 2008).

For nearly a decade, the consensus viewpoint had been that the first stars formed in isolation, between $30 - 300$ $M_\odot$ in mass, and only one per $\sim 10^6$ $M_\odot$ halo. This had been confirmed by divergent methods: both Smoothed Particle Hydrodynamics (SPH) simulations and Adaptive Mesh Refinement (AMR) calculations showed similar results (Abel et al. 2002; Yoshida et al. 2003; O'Shea & Norman 2007). However, recently aspects of this picture are being challenged. Advancements in the current generation of simulations have taken place in three primary areas. The first is that the effect of heating from the formation of molecular hydrogen via three-body reactions (Turk et al. 2011a) is now being taken into account; this will heat the gas during later stages of collapse and through thermal regulation of the accretion rate produce higher infall velocities onto the central core. The second aspect is related to the so-called "Courant myopia" of calculations proceeding to high densities. Because the Courant timescale becomes extremely short at high densities, out of necessity previous simulations stopped after the formation of the first high-density core. Recent simulations have followed accretion for up to several thousand years, using the numerical technique of sink particles, accreting Lagrangian particles representing protostars below the resolution limit of the simulation (Greif et al. 2011a; Clark et al. 2011; Stacy et al. 2010). While this approach allows to follow the calculations further in time it does lack the mathematical rigor that may allow one to prove the result to be correct. The final effect now being added is simply that of sampling: in the published literature, very few calculations had been performed; compared to the wealth of calculations of galaxy mergers, cluster formation, and so on, the sampling of Population III star formation was dramatically underserved, with only a handful of papers discussing even multiple simulations (see, e.g., O'Shea & Norman 2007).

These recent shifts have suggested that these halos have fragmented into either a small-number multiplicity of protostars (Turk et al. 2009; Stacy et al. 2010) or many small-mass pre-stellar objects (Clark et al. 2011; Greif et al. 2011a). However, none of these simulations have included the effects of magnetic fields in their calculations, nor have they self-consistently followed the growth of seed magnetic fields over the collapse and virialization of these first minihalos. Similarly, the fragmentation has been only studied for times of less than 1% of the accre-

matthewturk@gmail.com
[1] Columbia University
[2] NSF CI TraCS Postdoctoral Fellow
[3] Stanford University
[4] SLAC National Accelerator Laboratory

KIPAC, SLAC National Accelerator Laboratory, 2575 Sand Hill Road, Menlo Park, CA 94025

Work supported in part by US Department of Energy contract DE-AC02-76SF00515.

tion time scale of the massive stars being studied. It has been difficult to show whether possible early fragments would survive and not grow substantially in mass and simply merge with the central proto-star.

The influence of magnetic fields on the collapse of the first stars has received a renewed interest in recent years (Machida et al. 2008). Early numerical simulations (Xu et al. 2008) including the Biermann battery effect suggested that the dynamical effect of magnetic fields on primordial gas is very small. Though their resolution was rather low, these simulations found that fields were primarily built up by collapse, leading to $B \propto \rho^{2/3}$. The thermodynamics of primordial gas are quite sensitive to the $\mathbf{B} - \rho$ relationship via heating from ambipolar diffusion (Sethi et al. 2010). Although magnetic fields are believed to be unlikely to affect the characteristic fragmentation scale for Population III stars, they may increase the temperature in very high density gas, leading to higher accretion rates onto the protostars (Schleicher et al. 2009). The ability of turbulent fluid motions to drive dynamo action during primordial protostellar collapse has been predicted analytically by Schleicher et al. (2010) and confirmed numerically by Sur et al. (2010) and Federrath et al. (2011) for idealized collapse calculations. The latter work also suggested that a minimum resolution of 32 elements per Jeans length is required to capture dynamo action, giving a very strong motivation for higher resolution cosmological MHD calculations. Properly resolved, dynamo amplification leads to exponential growth of the field over a turbulent eddy turnover time, and can radically change the strength of the magnetic field at any given density during collapse. The Federrath et al. (2011) simulations considered the collapse of a nearly-isothermal Bonnor-Ebert sphere with turbulence seeded by velocity perturbations. While these conditions were idealized from earlier hydrodynamic cosmological computations, we seek a more complete picture by following the full magnetohydrodynamic (MHD) evolution of primordial gas from cosmological initial conditions. This allows us to self-consistently study the interaction of primordial gas dynamics, turbulence, and dynamo action.

In this paper, we present the first highly-resolved calculations of the formation of the first stars in the Universe from cosmological initial conditions, taking into account a full suite of chemical reaction rates, chemical heating due to three-body reactions, magnetic fields from primordial seed fields, and a resolution of 64 zones per Jeans length. Furthermore, it has been conducted with an open source, community-built simulation code available for inspection and contribution. In this paper, we examine both the large-scale and small-scale amplification of the magnetic field, as well as the manner in which resolution affects the chemo-kinetic state of the inner molecular cloud. A forthcoming paper will study the growth of turbulence in more detail.

2. METHODS AND SIMULATIONS

The simulations described in this work were conducted with the Enzo simulation code[5]. Enzo is an adaptive mesh refinement (AMR) simulation code, wherein the baryonic fluid is discretized onto an Eulerian grid. In cells where certain criteria are violated (such as overdensity, Jeans parameter, slopes of fluid quantities) higher resolution regions are inserted. This process is applied dynamically throughout the course of the simulation, ensuring adequate resolution of physical processes on all length scales – while the innermost regions of the calculation may evolve more quickly dynamically, the entire simulation is coupled and large-scale torques, inflow, and halo properties are self-consistently included.

They were initialized with cosmological initial conditions generated from Gaussian random noise, in a manner identical to that conducted in Abel et al. (2002); O'Shea et al. (2004); Turk et al. (2009, 2010). The parameters for generating the initial perturbations, as well as the partitioning of the matter budget into dark and baryonic components, have been taken from WMAP7 results (Jarosik et al. 2011). The simulations were initialized from a single random seed at a redshift of 99, with their simulation volume centered on the first massive halo to form in the simulation box, 8.5×10^5 $M_\odot$ at $z = 19.72$. For our initial conditions, we create a set of nested grids initialized from the primordial power spectrum, which are then allowed to dynamically refine as described below. The initial structure of our simulation was an outermost 128^3, 300 kpc h^{-1} (comoving) box, within which three subsequent, nested levels of refinement were initialized, for a final dark matter mass resolution of $2.3 M_\odot$ and a baryonic cell width of 290 pc h^{-1} (comoving). The highest-resolution region at time of initialization is a cube of side length of 75 kpc h^{-1} (comoving) and we allow further refinement during the course of the simulation within a cube of side length 12 kpc h^{-1} (comoving) centered on the most massive halo in the simulation at a redshift of 20.

To solve the cosmological magnetohydrodynamic equations, we use the HLL Riemann solver with piecewise linear reconstruction. The $\nabla \cdot \mathbf{B} = 0$ constraint is enforced using the Dedner scheme (see Wang et al. 2008, 2010, for a full description). We have utilized a lower-order chemical solver than previous studies; in both Turk et al. (2010, 2009) a solver based on the work of Verwer (1994) was used. Here we have used a modified version of the solver from Anninos et al. (1997), in the interest of quantifying the influence of the magnetic field on the overall collapse, as well as the growth of the magnetic field. This choice of chemistry solver results in less finely-balanced equilibrium between molecular hydrogen formation and dissociation. Despite that, as discussed below, there are substantial differences in the molecular hydrogen fraction in these calculations, as well as the temperature, as a function of resolution. We have included the formation heating from molecular hydrogen (4.48 eV), and have used the Glover (2008) three-body formation rate. Recent works (Naoz et al. 2011; Greif et al. 2011b) have suggested that relative velocities between the baryonic matter and dark matter may affect the details of early structure formation; we do not include those effects here, although this issue remains an important one to address in future simulations.

We have conducted four simulations, each of which vary only in the parameters governing the AMR algorithm. Typically in AMR calculations of the first stars

[5] `http://enzo-project.org/`, described in Bryan & Norman (1997); O'Shea et al. (2004), conducted with changeset `f3cf4f13e195`

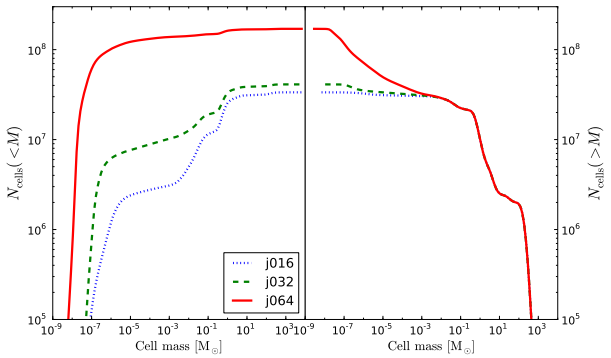

FIG. 1.— A plot of the number of cells as a function of mass enclosed in those cells, for each of the simulations at the time at which the simulations were terminated, at a peak density of 10^{-10} g cm^{-3}, the time at which all analysis in this paper was conducted. J16 is represented in dotted blue, J32 in dashed green, J64 in solid red. This cell count is cumulative; on the left we show the total number of cells with mass less than the x-axis value, and on the right we show all cells with mass greater than the x-axis value.

in the universe, Jeans resolution is the dominant refinement criteria. The four simulations presented in this work vary in the number of cells mandated to resolve the Jeans Length in each direction; we have conducted simulations requiring 16, 32, 64 and 128 cells in each direction, named J16, J32, J64 and J128. In all simulations, rather than calculate the Jeans length from the local temperature, we calculated it assuming that the gas would be allowed to cool to 200 K, as in Turk et al. (2010), which provides substantially better resolution of higher-temperature gas. We additionally require refinement on relative overdensities; at the coarsest level, we flag zones that are four times the mean density, and with each additional level this decreases by a factor of $2^{-0.3}$. This provides the refinement at scales larger than the virial radius, inside which refinement based on Jeans criteria dominates. These simulations began from the same initial conditions and were seeded with an identical uniform magnetic field of 10^{-14} G (proper), corresponding to a comoving magnetic field of 10^{-18} G at the start of our calculation. With the exception of J128, these simulations were terminated at a peak density of 10^{-10} g cm^{-3}; in the case of J128, we terminated the simulation at a peak density of 10^{-19} g cm^{-3}. We chose this density as it was the point at which the simulation ceased to be feasible on available computational resources, and at which we were able to demonstrate the variation in magnetic field amplification discussed below; future studies will utilize this level of resolution, and potentially higher, for calculations of Population III star formation. In Figure 1 we plot the number of cells in each simulation as a function of the mass enclosed in that cell; for J64, we note that we have 1.4×10^8 cells containing mass less than 10 times the mass of the Earth.

3. RESOLUTION EFFECTS IN GAS DYNAMICS

The gas dynamics of these collapsing clouds is substantially modified by both increased resolution and the indirect consequences of those resolution-dependent effects. By directly comparing the three mature calculations (J16, J32, J64) at identical peak-density times, we quantify these differences. In particular, the differences in the chemical, kinetic, and thermal states of the gas are the most pressing, as they will directly relate to the potential for fragmentation at later times. Because these simulations are stopped before the formation of the first hydrostatic core, and more importantly before that hydrostatic core has undergone several mass doublings, we do not use these data sets to estimate the initial mass function of the first stars, and instead confine our comments to measurable environmental effects and their potential consequences for magnetic field amplification, gravitational instability, and the subsequent accretion onto the central molecular cloud.

3.1. *Resolution dependence of T and H_2 and v_r*

In the collapse of Population III stars, the chemical and thermal states of the gas have been shown to be important when considering the accretion rates and potential fragmentation (Abel et al. 2002; O'Shea & Norman 2007; Clark et al. 2011; Greif et al. 2011a; Turk et al. 2010, 2009). In particular, recent findings from Turk et al. (2011a) suggest that the character and quantity of fragmentation in metal-free collapsing halos may depend strongly on the behavior of molecular hydrogen at high densities.

As molecular hydrogen forms via three-body reactions (where typically the third body is either another atom of hydrogen or a molecule of hydrogen) the 4.48 eV binding energy is released into the surrounding gas in thermal energy, via collisional deexcitation. During the collisional dissociation of molecular hydrogen through the inverse reactions to the three-body rates, the binding energy is removed from the thermal energy of the gas. Clark et al. (2011) proposes this as a mechanism for retaining isothermality in collapsing halos; as primordial gas reaches densities above 10^{-8} g cm^{-3}, it becomes optically thick to all efficient radiative cooling until the gas reaches at least 6000 K. This is proposed as a mechanism for allowing the gas to fragment under gravitational instability. This method of fragmentation relies heavily on the chemical state of the molecular cloud at high densities, and would be sensitive to a lower molecular hydrogen fraction, as this would impede gravitational instabilities from retaining isothermality and thus serving as a channel for spontaneous fragmentation.

In Figure 2 we show spherically-averaged radial profiles, computed at the final output and centered at the densest zone in the calculation, of density, temperature, radial velocity, molecular hydrogen mass fraction, vorticity and enclosed mass as a function of radius. The central velocity was subtracted before calculation of the radial velocity. As a function of radius, we see good agreement between J16, J32 and J64 at radii greater than 10^{19} cm in the density profile. However, at approximately 3×10^{18} cm (~ 1 pc) we see a small bump in the J16 and J32 runs. This is not present in the J64 runs. Typically bumps in the density plot indicate the formation of a second clump or other moderate level of fragmentation; however, based on the length and density scales here, we attribute this to poor resolution in the lower-resolution runs contributing to a spike of unresolved clumping just inside the virial scale; we also note that it correlates directly with the lowest infall velocity in all three simulations, so it may also simply be material that is being processed into the inner regions of the halo.

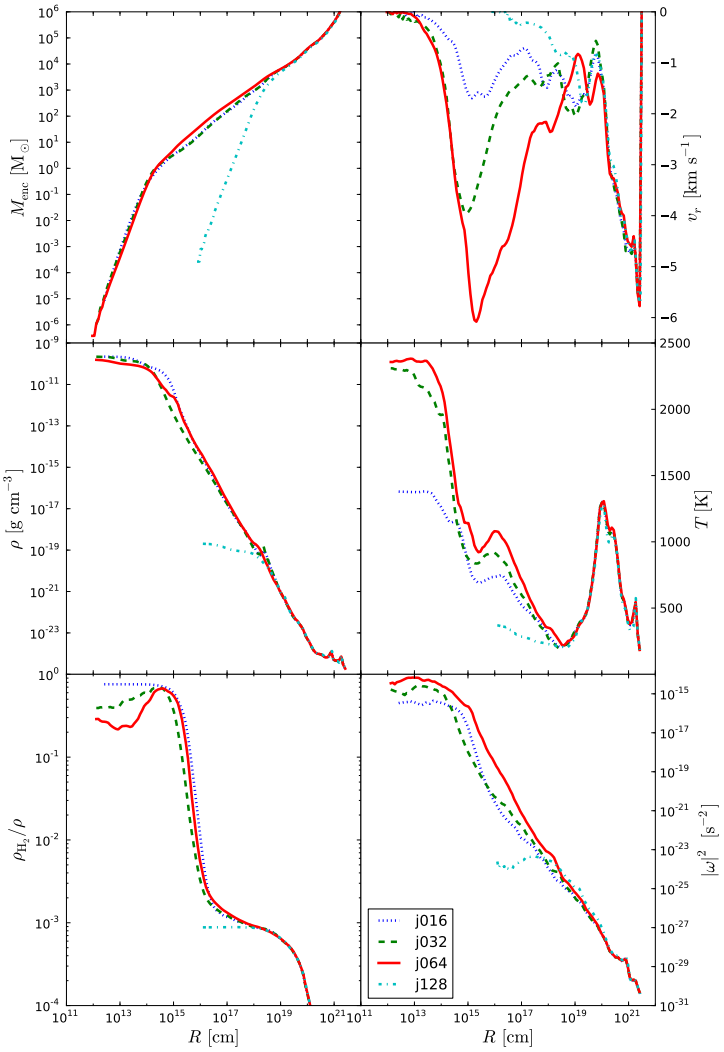

FIG. 2.— Radially-binned, spherically-averaged radial profiles of the four simulations taken at their final output. These profiles were centered at the most dense point; J16 is dotted blue, J32 is dashed green, J64 is solid red, and J128 is dot dashed cyan. Note that we terminated J128 before it reached the same peak density as the other simulations, although J16, J32 and J64 were terminated at roughly identical peak densities. Upper left is the total mass enclosed (in solar masses) at a given radius, upper right is the radial velocity in km s^{-1}, middle left is the density inside a given radial bin in g cm^{-3}, middle right is the temperature in K, bottom left is molecular hydrogen mass fraction, and bottom right is the magnitude of the local vorticity.

The changes in the chemical and kinetic states of the gas as a function of resolution are clearly correlated; with increased resolution, the infall velocity increases, as does the corresponding temperature, causing a direct decrease in the overall molecular hydrogen fraction. While we still see a peak in the molecular hydrogen, corresponding to a molecular hydrogen cloud of about $1-5$ M$_\odot$, the J64 run has substantially lower molecular hydrogen fraction of $\sim 0.2-0.3$ in the innermost core, versus nearly twice that for J32 and approximately unity in the J16 case. As is to be expected, this correlates strongly with the thermal state of the gas; while J16 has a peak temperature of approximately 1400K, the J32 and J64 cases both exceed 2000K (with J64 reaching 2400K.) The rate at which molecular hydrogen is collisionally dissociated steeply depends on temperature, and the relationship between these two quantities has been explored previously Turk et al. (2011a). With increased resolution the homogeneity of the chemical and density structure of the cloud cloud decreases, but we see more morphological homogeneity, as discussed below.

The radial velocity structure remains roughly the same between all three simulations, although the magnitude of the infall velocity increases with increased resolution. In the J16 case, we see an infall velocity at the radius of the edge of the molecular cloud of approximately 2 km/s, although this increases to 6 km/s in the J64 case. The J32 case is in between these two. The J16 case shows slight peaking, indicating an under-resolved shock at the exterior of the molecular region, but both J32 and J64 show very strong shocking structures. When compared to the enclosed mass, we see that J64 encloses a factor of ~ 1.5 as much mass at a given radius inside the virial radius. This likely contributes to this much greater buildup in shock. Furthermore, the increased resolution will allow much finer shocking surfaces to develop and to be

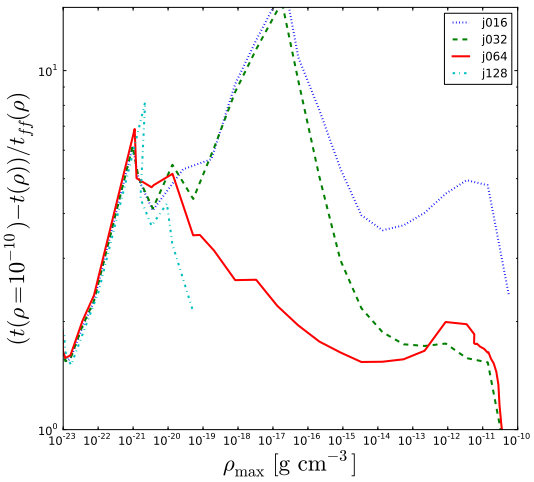

FIG. 3.— The differential free-fall time for all four simulations, J16 (dotted blue), J32 (dashed green), J64 (solid red) and J128 (dashed-dotted cyan, which has not reached the same peak density) The x-axis corresponds to a given density; the values along the y-axis have been calculated by subtracting the time at which the simulation was at a given peak density from the time at which the simulation had a peak density of of 10^{-10} g cm^{-3}, then dividing by the differential free-fall time scales between the two times. Higher-values therefore correspond to a longer collapse time, and lower-values correspond to a shorter collapse time with respect to the free-fall time.

resolved (a noted problem with under-resolved hydrodynamics.)

3.2. *Timescales of Collapse*

Ideally, in the course of a resolution study the basis for comparison between two otherwise identical calculations would be comparison at a fixed time. However, this method is not possible in full cosmological simulations because the hydrodynamics of the calculation are greatly influenced by resolution effects both directly, through turbulent stirring of the gas, viscosity, and numerical diffusion effects, and indirectly through variations in the chemical state of the gas as a result of temperature and turbulence differences.

In lieu of direct comparisons against identical times since the Big Bang, we have conducted our analysis against identical peak density times. While this neglects time dependencies such as the growth of mass at the innermost shocking region, the velocity structure variations with time in the molecular cloud and so on, it does provide a baseline for comparing the chemical and kinetic state within the free-falling core. In particular, this is the same technique utilized in Turk et al. (2011a).

To account for variations, we present in Figure 3 a visualization of the variations in the timescale of collapse and the freefall timescale for each calculation. Higher values correspond to a differential collapse time compared to expected freefall timescales; one can clearly see that simulations J16 and J32 are much slower to collapse than J64 at all densities less than 10^{-13} g cm^{-3}, at some densities even reaching ten times the freefall timescale. In particular, the peak delay for simulations J16 and J32 occurs at a density of roughly 10^{-17} g cm^{-3}, the density at which (as discussed above in § 3.1) molecular hydrogen begins forming via the three-body reaction, and therefore marking the edge of the molecular cloud. Furthermore, as noted below, the morphological differences between the three simulations indicate that this is correlated with variations in morphology.

3.3. *Morphological Differences*

In Figure 4 we show density-weighted density projections of the final output from the calculations. From left, these show the J16, J32 and J64 calculations, and from the top they have field of view of 300 pc, 1 pc, and 1000 AU. The most striking difference between the simulations is found in the morphology. Only one (J16) of the three simulations that reached 10^{-9} g cm^{-3} (J16, J32, J64) has formed a clear disk, with two spiral arms. Both J32 and J64 have not yet formed a disk, and both show obvious cloud-like morphology, with J64 exhibiting somewhat ellipsoidal morphology. While J64 will form an accretion disk at a later time, the variation in the settling times is striking, particularly as the time at which an initial protostar ignites and irradiates its surroundings will alter the environment for the potential formation of subsequent protostars. Furthermore, the dramatic differences in the morphology suggest that resolution directly impacts the formation environment, and may influence the gravitational stability of a collapsing cloud.

In Figure 5 we plot density-weighted projections of the molecular hydrogen mass fraction from the same outputs and with the same field of views as in Figure 4. We note in particular that the morphology of the molecular hydrogen cloud roughly tracks the overall density structure; however, the molecular cloud in the J16 simulation is substantially larger than those in the J32 and J64 calculations. This can be seen in Figure 2, wherein the J16 calculation has a slightly larger molecular cloud when averaged radially. Furthermore, while not obvious here owing to the density-weighting, the innermost regions of J32 and J64 show molecular hydrogen fractions of ≤ 0.4, and even as low as 0.2 in J64. In J16, the molecular hydrogen cloud tracks almost identically the spiral arms in density; at the leading and trailing ends the fraction drops. This occurs because, as the three-body reaction for forming molecular hydrogen is strongly density-dependent. The increased cooling properties with higher molecular hydrogen fraction will only exacerbate this distinction between the spiral arms and the medium of the disk, spurring further collapse. In the J32 and J64 runs, we see not only highly-irregular, spheroidal structure, but we see little to no evidence for runaway gravitational instability at this time in the collapse; in fact, the roughly spheroidal structure of the cloud suggests that disk fragmentation at the ~ 100 AU scale may be disfavored, certainly until a later time.

4. MAGNETIC FIELD AMPLIFICATION

We infer magnetic field amplification above that arising simply from the spherical compression of frozen-in field lines during collapse by plotting the magnetic energy, $E_B = B^2/8\pi$, as a function of density for each of our four simulations (figure 6). Assuming a power law relation between magnetic energy and density, $E_B \propto \rho^b$, a spherical collapse would result in $b = 4/3$. Any steeper values of b must result in additional amplification in the form of a dynamo. We expect a small-scale turbulent

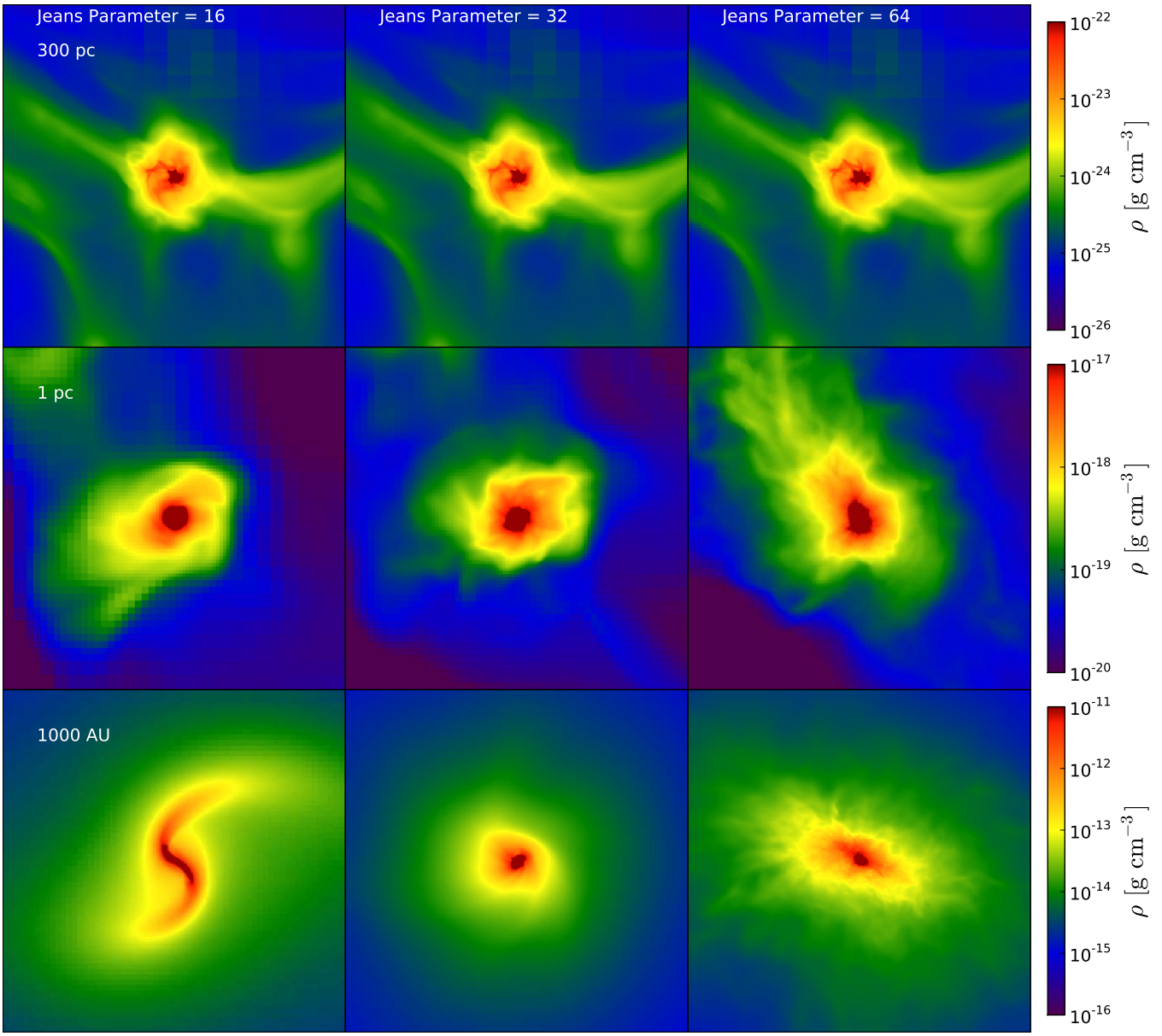

FIG. 4.— Density-weighted projections (through the entire simulation domain) of the average density field in simulations J16 (left column), J32 (second column) and J64 (third column) at fields of view of 300 pc (top row), 1 pc (middle row), and 1000 AU (bottom row).

dynamo if there is significant kinetic energy in turbulent motions. Figure 6 shows that for the best resolved simulations, J64 and J128, the magnetic field scales with a much higher power, $b \simeq 1.78$ at all densities $\rho \gtrsim 10^{-26}$, roughly consistent with the findings of Federrath et al. (2011). By contrast, the lower resolution runs (J16 and J32) begin to show $b > 4/3$ behavior at the same density as the higher resolution runs, but never reach the same b as the higher runs and eventually begin to show a shallower slope of E_B with ρ at the highest densities ($\rho \gtrsim 10^{-15}$). In the outer part of the collapse, near the virial radius, all runs show $b \simeq 4/3$, suggesting that at low densities, the growth of magnetic energy is primarily due to the roughly spherical collapse, though the data is somewhat scant.

4.1. *Velocity Structure In the Collapse Region*

The dynamo activity in the previous section is resolution dependent, but robust above roughly 64 cells per Jeans length (J64); that is, we continue to see more field amplification, consistent with a minimum resolution requirement of between 32 and 64 zones per Jeans length. This is broadly consonant with the results of Federrath et al, who find a similar resolution cutoff in their simulations of magnetic field growth in the nearly-isothermal collapse of a Bonnor-Ebert sphere. In their picture, the reason for this cutoff is the lack of sufficient power in rotational motions when the Jeans length is resolved with fewer than ~ 30 cells. Our resolution requirement for strong and sustained dynamo action appears to be about a factor of two larger, which could be due to our use of a considerably more diffusive MHD solver (we use the HLL solver; they use HLL3R). In order to solidify the connection between dynamo action and the presence or absence of turbulent fluctuations, we first consider pro-

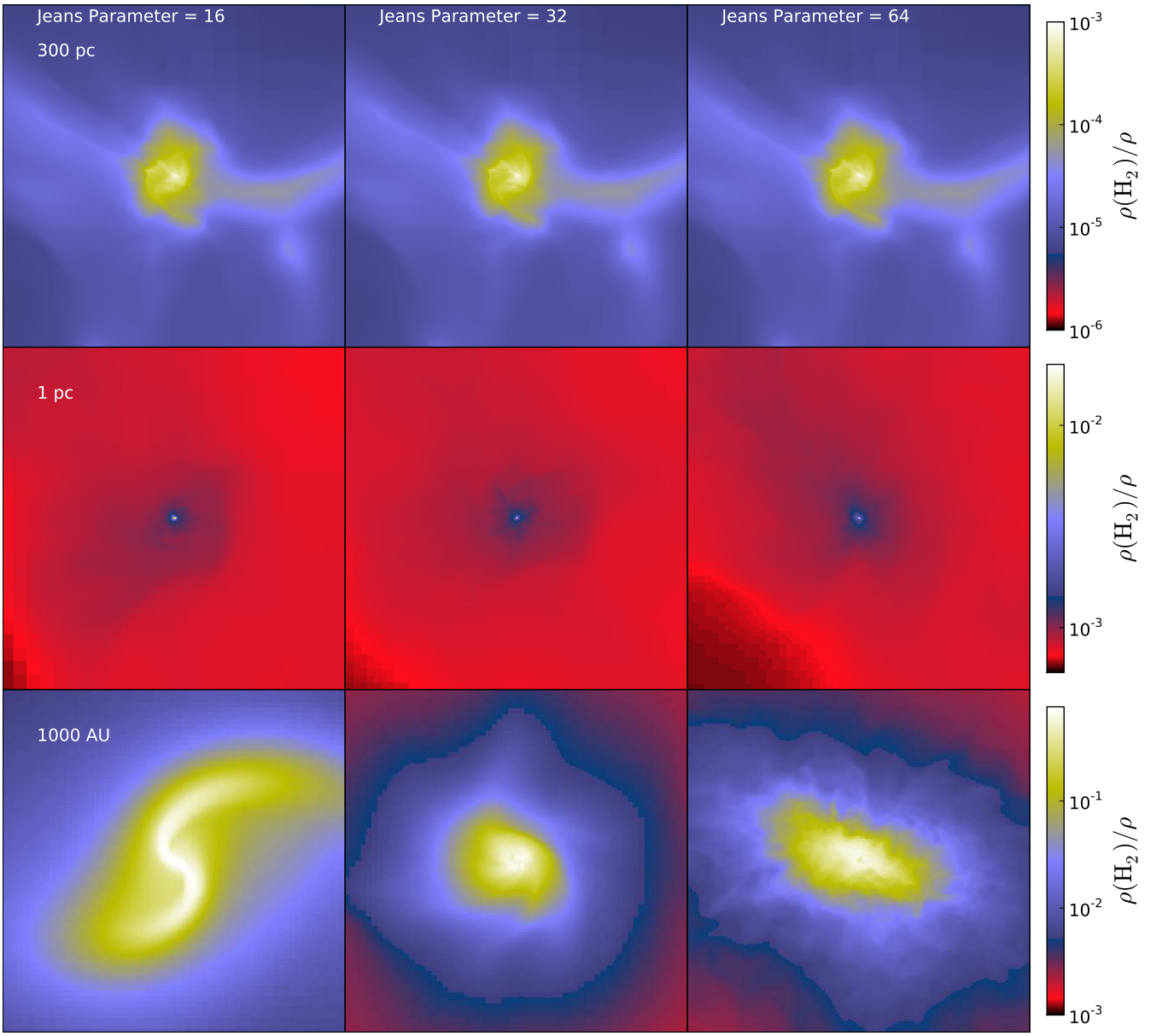

FIG. 5.— Density-weighted projections (through the entire simulation domain) of the average molecular hydrogen mass fraction field in simulations J16 (left column), J32 (second column) and J64 (third column) column) at fields of view of 300 pc (top row), 1 pc (middle row), and 1000 AU (bottom row).

jections of ω^2 where $\omega = \nabla \times \mathbf{v}$ is the fluid vorticity centered at the densest point in the computation (figure 8). At the 300pc scale (figure 8, top row), the vorticity is identical among the four resolutions. However, zooming in to $\sim$ 1pc, there are already significant differences between all four runs. For the other three, a trend is clear: increasing resolution creates much larger regions of high vorticity that is indicative both of an overall increase in the turbulent energy but also of a decreasing coherence of the collapse region (see section 3.3). Finally, at 1000AU, the vorticity structure is completely different between the ordered disk-like structure in J16 and J32 and the amorphous turbulent core of J64. It is thus clear that as a function of resolution, we see an increase in vorticity production and a decrease in the characteristic scale of that vorticity at the smallest scales within the collapsing core. These high density regions are just where magnetic energy growth with density begin to fall off in low resolution simulations. This correlation between vorticity and magnetic energy is consistent with small-scale dynamo action generated by incoherent velocity fields.

4.2. *Magnetic Field Saturation*

The kinematic, small-scale dynamo acts by twisting magnetic field in a turbulent flow field. The random-walk character of the flow will lead to a continuous stretching and thus strengthening of the magnetic field. In a typical numerical model of the small-scale dynamo, turbulence is driven in a fluid with a tiny seed field; the field grows exponentially until it nears equipartition with the turbulent velocity field, at which point the Lorentz force reacts back on the fluid, leading to a strongly nonlinear coupling between $\mathbf{v}$ and $\mathbf{B}$ which ultimately saturates the growth of the magnetic field.

Here, the collapse timescale is decreasing with time,

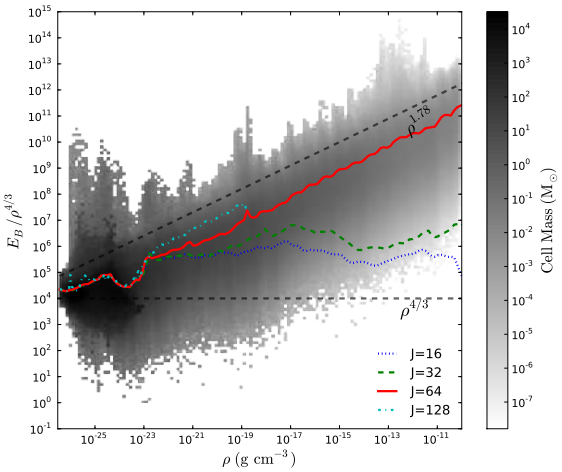

FIG. 6.— Lines show volume-weighted magnetic energy scaled by $\rho^{4/3}$ as a function of density for a $1-$kpc sphere centered on the densest point in the final output for each of four resolutions, J16, J32, J64, and J128. The colored pixels give the mass in $E_B-\rho$ bins for the J64 run. We have overlaid two power laws, giving $B \propto \rho^{4/3}$ (lower dashed line), the expected scaling for spherical collapse of frozen-in magnetic fields, and $B \propto \rho^{1.78}$ (upper dashed line), the best-fit power law to the J64 data.

which means that the computation reaches its end long before the magnetic field reaches saturation. We stop each of our runs when their peak density is $\rho_{max} \simeq 2.2 \times 10^{-10}$, except for the J128 run, which was terminated at $\rho_{max} \simeq 2.0 \times 10^{-19}$ due to constraints on computing time. Nevertheless, even in the J64 run, where dynamo action is most vigorous, the kinetic energy exceeds the magnetic energy in mass weighted averages by a factor of ~ 3600.

The growth rate σ of the small-scale dynamo is a function of the Reynolds number Re, the ratio of the advective timescale to the viscous timescale, which we do not control in these runs (dissipation is solely a numerical artifact of finite resolution). (Federrath et al. 2011, see, e.g.,) found the growth rate to be $\sigma \propto \mathrm{Re}^{0.3}$. Even if we were to solve the Navier-Stokes equation including viscosity and the non-ideal induction equation including Ohmic resistivity, we would be nowhere near the actual Reynolds numbers of the flows in primordial gas. A rough estimate of Re using the Spitzer viscosity, characteristic velocity and length scales taken from Figure 2 is about $\mathrm{Re} \sim 10^{12}$ at a radius of ~ 1000 AU . This means that our simulations cannot make a definitive statement regarding the saturation level of the collapse dynamo, though our results can be taken as a lower limit to the field strength during collapse. We note that this indicates that magnetic fields may be dynamically important in the formation of the first stars, and that their amplification requires much higher resolution than is currently being utilized.

5. DISCUSSION

It is clear from our simulations that gravitational collapse from cosmological initial conditions does indeed drive a small-scale dynamo if the flow is resolved well enough to capture the turbulent fluctuations. This turbulence is produced self-consistently by the collapse dynamics, and is not seeded by any driving or initial perturbations. The change in slope between J64 and J128 indicates that while we have demonstrated the minimum resolution for dynamo action to occur, further amplification of the magnetic field will result from increased resolution, and thus our results should not be considered converged. We will explore the details of the generation the turbulence and the details of the dynamo generated magnetic field in a forthcoming paper.

The most striking difference between the J16, J32 and J64 runs is the resolution-dependence in the chemical and kinetic states of the gas. While we initially expected that the simulations would produce largely the same results in the structure of the collapsing clouds, the three simulations produced substantially different disk structure. Because we examined these three simulations at identical peak density values, the time remaining until the formation of the first hydrostatic core should be roughly identical in each run; as such, the initial structure of the cloud will likely not change in that intervening time. Clark et al. (2011) presented simple comparisons between the accretion rate onto the central accretion disk and the accretion rate onto a central protostar; in those calculations these comparisons indicate that the central core will be unable to process sufficient gas to deplete the disk, which they observed result in gravitational instability. We note that in our simulations, we see substantially reduced disk-like structure, as well as substantially higher infall velocities at the edge of the molecular hydrogen cloud. The combination of these two effects results in an unclear change to the potential fragmentation characteristics of these collapsing clouds; reduced angular momentum should allow greater accretion onto a central core, but the increased radial velocity onto the molecular cloud will result in greater mass-buildup. Furthermore, we note that while we do not resolve the formation of a central core or the subsequent accretion, and thus cannot make statements regarding the fragmentation characteristics in our simulation, the result presented in Clark et al. (2011) was constructed from a series of fixed resolution calculations with a much lower Jeans resolution than in our J64 run (and indeed our J32 run); the results in this paper suggest that higher resolution may change the specific nature of fragmentation.

The correlation between the dissociation of molecular hydrogen and the increased resolution was unexpected, but in retrospect is not entirely surprising. With increased infall velocity, increased turbulent support, and increased overall temperature, the rate at which molecular hydrogen collisionally dissociates increases steeply, while the rate at which it associates via three-body reactions decreases. With increased turbulent energy, and a corresponding increase in the temperature, the innermost region in the pre-stellar molecular cloud will naturally undergo some dissociation. However, what remains unclear is how this will affect the response of the gas to gravitational instability. Prior to the work of Clark et al. (2011); Greif et al. (2011a), fragmentation had been seen at scales of $\sim$ 2000 AU (Turk et al. 2009; Stacy et al. 2010); at smaller scales, fragmentation had (prior to the works of Clark, Greif and their collaborators) been believed to be suppressed because of the inefficient cooling of molecular hydrogen. In these more recent works, however, the ability of the gas to shed thermal energy through dissociation of molecular hydrogen, essentially

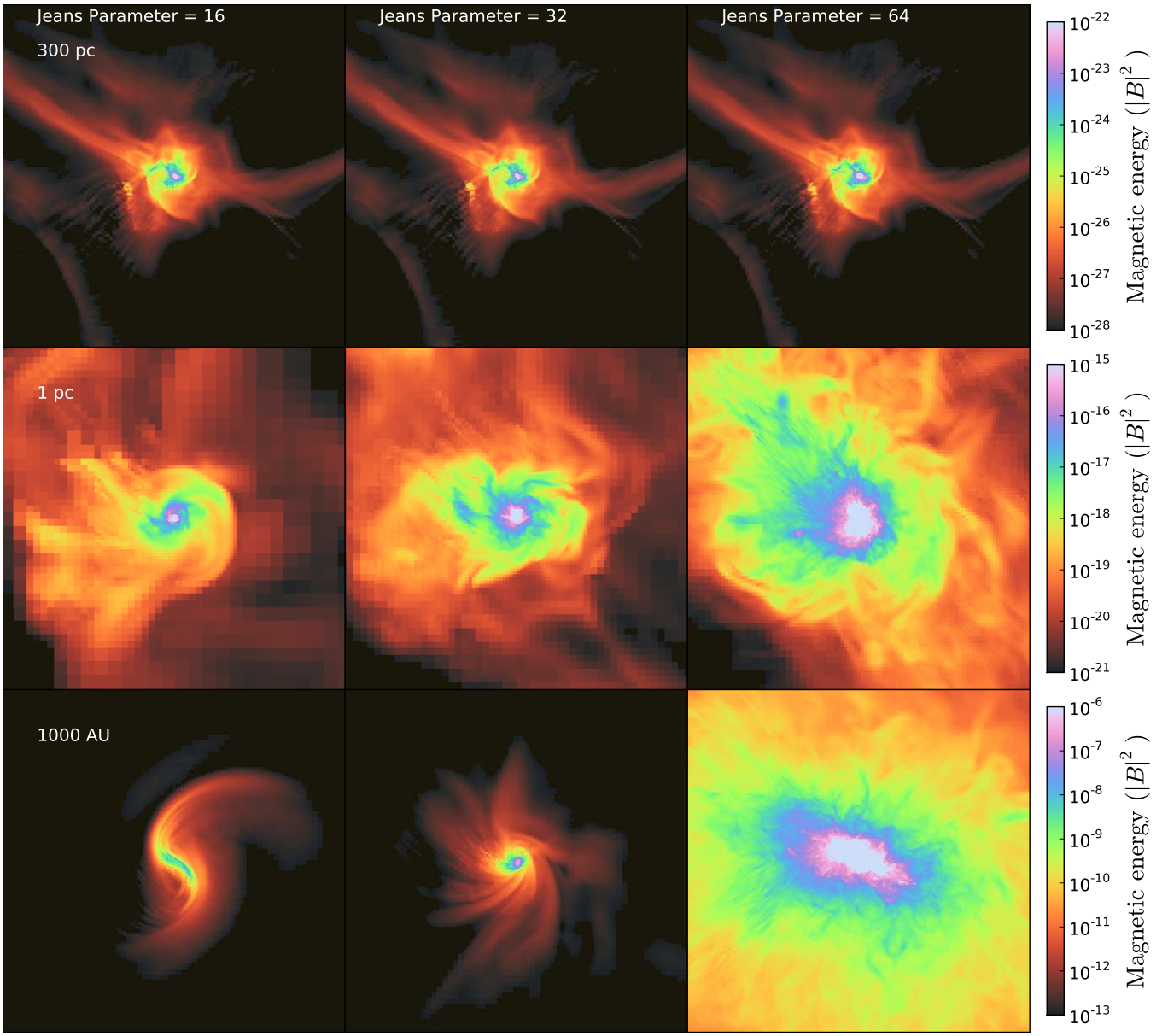

FIG. 7.— Density-weighted projections (through the entire simulation domain) of the average magnetic energy in simulations J16 (left column), J32 (second column) and J64 (third column) at fields of view of 300 pc (top row), 1 pc (middle row), and 1000 AU (bottom row).

allowing compressional heating to be freely reversed, has been identified as the mechanism by which fragmentation proceeds. At high densities (the densities at which sink particles have been inserted in their calculations), the gas becomes effectively isothermal (and later, once the molecular hydrogen has been depleted, adiabatic.) However, this hypothesis relies on a substantial reservoir of molecular hydrogen; while a gas cloud containing a depleted but non-zero supply of molecular hydrogen is still likely to undergo a quasi-isothermal phase during its collapse, the resilience of that gas and the stiffness of its effective equation of state are likely to be modified. Furthermore, because the fraction of molecular hydrogen, and thus the equation of state of potentially-fragmenting gas sensitively depends on the rate at which molecular hydrogen is formed and destroyed, as discussed in Turk et al. (2011a), this provides an additional uncertainty. Without extremely high-resolution calculations that follow the formation of the first core, as well as its subsequent accretion over several thousand years, the character of fragmentation in accretion disks around Population III pre-stellar cores is still an open question.

6. CONCLUSIONS

We have presented on the first fully-cosmological calculations of Population III star formation that include all relevant chemical processes, as well as magnetic fields. We see, in agreement with Federrath et al. (2011), that a critical resolution exists above which we are able to resolve small-scale dynamo action resulting in increased magnetic-field field growth. While we adequately resolve the *action* of this small-scale dynamo, we have not yet resolved the amplification caused by that dynamo, as demonstrated by the nascent J128 simulation. In fact, while these calculations have yet to show a dynamically-important magnetic field, estimates of the possible sat-

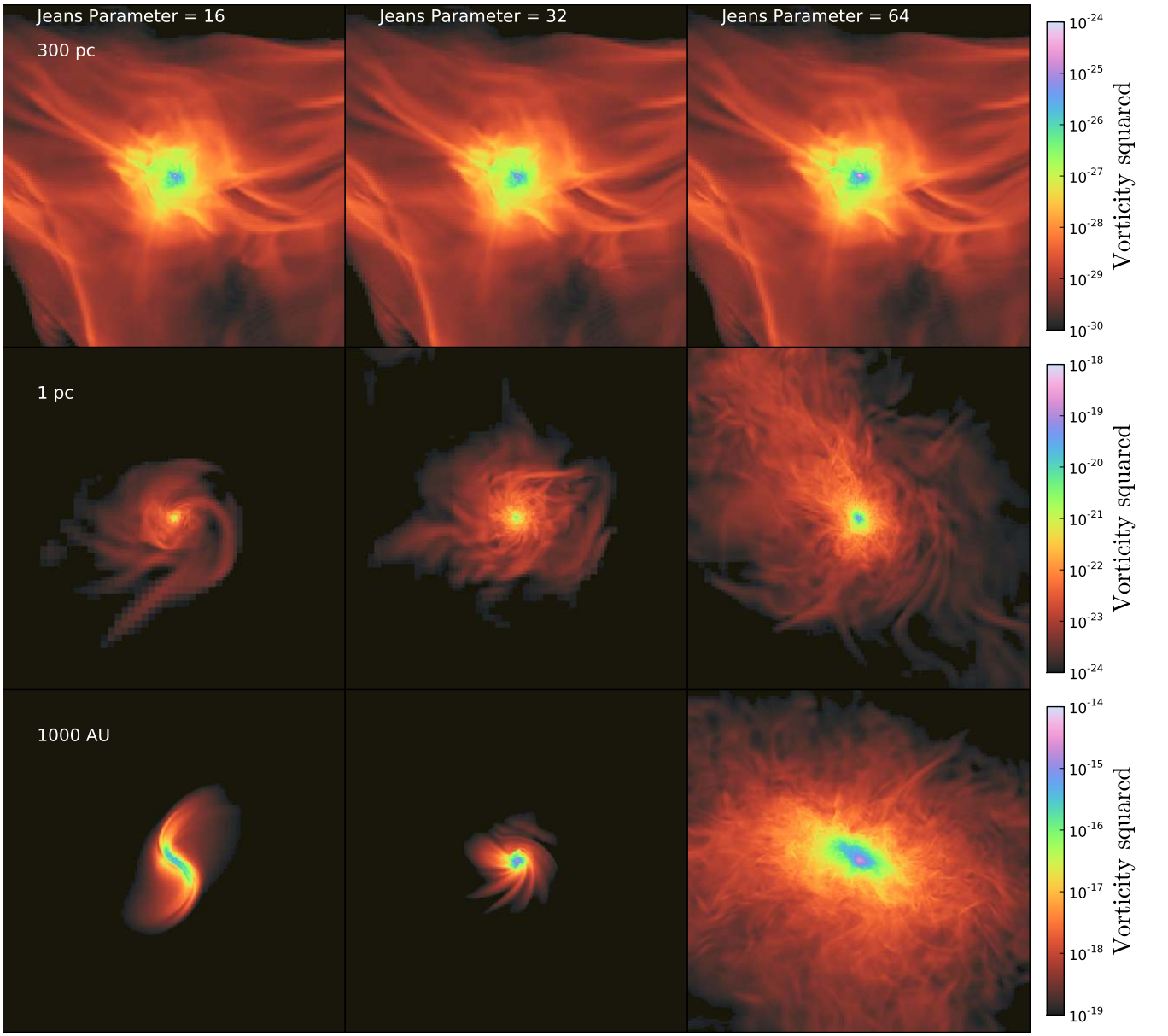

FIG. 8.— Density-weighted projections (through the entire simulation domain) of the average magnitude of the local vorticity in simulations J16 (left column), J32 (second column) and J64 (third column) at fields of view of 300 pc (top row), 1 pc (middle row), and 1000 AU (bottom row).

uration level of the magnetic field indicate that with increased resolution or stronger seed fields, magnetic fields may in fact become dynamically important.

A side effect of conducting these resolution studies has been that we see substantial variation in the chemical, kinetic, and velocity structure of collapsing metal-free, star-forming clouds. In particular, the substantial difference in the J64 run suggests that under-resolving the hydrodynamics can result in incorrect solutions: the fraction of hydrogen gas that is in molecules, the speed of sound, the infall velocity and the turbulent support all depend strongly on hydrodynamic resolution.

Our calculations, while falling short of following potential fragmentation in detail, suggest that resolution effects may be an additional complication in determining the initial mass function of the first stars; in fact, they suggest that previous calculations in the literature have not yet converged on a solution. Future calculations, of much higher resolution and attaining a greater saturation level of magnetic fields, will help to resolve these outstanding questions.

M.J.T. acknowledges support by the NSF CI TraCS fellowship award OCI-1048505. This material is based upon work supported by the National Science Foundation under a grant awarded in 2010. G.L.B. acknowledges support from NSF grants AST-0547823, AST-0908390, and AST-1008134, as well as computational resources from NASA, the NSF Teragrid, and Columbia Universitys Hotfoot cluster. The simulations were run at the SLAC National Accelerator Laboratory, on the computing cluster orange. We are grateful for the support of the scientific computing department at SLAC as well as to Stuart Marshall's patient assistance with file system

and cluster issues. All analysis was conducted using `yt` (Turk et al. (2011b), `http://yt-project.org/`). We thank the anonymous referee for useful comments.

REFERENCES

Abel, T., Anninos, P., Zhang, Y., & Norman, M. L. 1997, New Astronomy, 2, 181
Abel, T., Bryan, G. L., & Norman, M. L. 2002, Science, 295, 93
Anninos, P., Zhang, Y., Abel, T., & Norman, M. L. 1997, New Astronomy, 2, 209
Bryan, G. L., & Norman, M. L. 1997, ArXiv Astrophysics e-prints (arXiv:astro-ph/9710187)
Caffau, E., Bonifacio, P., François, P., et al. 2011, Nature, 477, 67
Clark, P. C., Glover, S. C. O., Smith, R. J., et al. 2011, Science, 331, 1040
Federrath, C., Sur, S., Schleicher, D. R. G., Banerjee, R., & Klessen, R. S. 2011, ApJ, 731, 62
Frebel, A., Aoki, W., Christlieb, N., et al. 2005, Nature, 434, 871
Frost, M. I., Surace, J., Moustakas, L. A., & Krick, J. 2009, ApJ, 698, L68
Glover, S. 2008, in American Institute of Physics Conference Series, Vol. 990, First Stars III, ed. B. W. O'Shea, A. Heger, & T. Abel, 25–29
Glover, S. C. O., & Abel, T. 2008, MNRAS, 388, 1627
Greif, T. H., Springel, V., White, S. D. M., et al. 2011a, ApJ, 737, 75
Greif, T. H., White, S. D. M., Klessen, R. S., & Springel, V. 2011b, ApJ, 736, 147
Jarosik, N., Bennett, C. L., Dunkley, J., et al. 2011, ApJS, 192, 14
Machida, M. N., Matsumoto, T., & Inutsuka, S.-i. 2008, ApJ, 685, 690
Naoz, S., Yoshida, N., & Gnedin, N. Y. 2011, ArXiv e-prints (arXiv:1108.5176)
O'Shea, B. W., Bryan, G., Bordner, J., et al. 2004, ArXiv Astrophysics e-prints (arXiv:astro-ph/0403044)
O'Shea, B. W., & Norman, M. L. 2007, ApJ, 654, 66
Ripamonti, E., & Abel, T. 2004, MNRAS, 348, 1019
Schleicher, D. R. G., Banerjee, R., Sur, S., et al. 2010, A&A, 522, A115+
Schleicher, D. R. G., Galli, D., Glover, S. C. O., et al. 2009, ApJ, 703, 1096
Sethi, S., Haiman, Z., & Pandey, K. 2010, ApJ, 721, 615
Stacy, A., Greif, T. H., & Bromm, V. 2010, MNRAS, 403, 45
Sur, S., Schleicher, D. R. G., Banerjee, R., Federrath, C., & Klessen, R. S. 2010, ApJ, 721, L134
Turk, M. J., Abel, T., & O'Shea, B. 2009, Science, 325, 601
Turk, M. J., Abel, T., & O'Shea, B. W. 2008, in American Institute of Physics Conference Series, Vol. 990, First Stars III, ed. B. W. O'Shea, A. Heger, & T. Abel, 16–20
Turk, M. J., Clark, P., Glover, S. C. O., et al. 2011a, ApJ, 726, 55
Turk, M. J., Norman, M. L., & Abel, T. 2010, ApJ, 725, L140
Turk, M. J., Smith, B. D., Oishi, J. S., et al. 2011b, ApJS, 192, 9
Verwer, J. G. 1994, SIAM J. Sci. Comput, 15, 1243
Wang, P., Abel, T., & Kaehler, R. 2010, New Astronomy, 15, 581
Wang, P., Abel, T., & Zhang, W. 2008, ApJS, 176, 467
Wise, J. H., & Abel, T. 2005, ApJ, 629, 615
Xu, H., O'Shea, B. W., Collins, D. C., et al. 2008, ApJ, 688, L57
Yoshida, N., Abel, T., Hernquist, L., & Sugiyama, N. 2003, ApJ, 592, 645
Yoshida, N., Omukai, K., & Hernquist, L. 2008, Science, 321, 669